Air-Stable High-Efficiency Solar Cells Using Improved Single-Walled Carbon Nanotube Films

Kehang Cui,[1] Anton S. Anisimov,[3] Takaaki Chiba,[1] Shunjiro Fujii,[4] Hiromichi Kataura,[4] Albert G. Nasibulin,[2] Shohei Chiashi,[1] Esko I. Kauppinen,[2] Shigeo Maruyama[1]

[1] Department of Mechanical Engineering, The University of Tokyo, Bunkyo-ku, Tokyo 113-8656, Japan

[2] Department of Applied Physics, Aalto University School of Science, Aalto FI-00076, Finland

[3] Canatu Ltd., Konalankuja 5, FI-00390 Helsinki, Finland

[4] Nanosystem Research Institute, National Institute of Advanced Industrial Science and Technology, Tsukuba 305-8562, Japan

Corresponding Author:

Shigeo Maruyama, maruyama@photon.t.u-tokyo.ac.jp,
Department of Mechanical Engineering, The University of Tokyo, 7-3-1 Hongo, Tokyo, 113-8656, Japan; Tel: +81-3-5841-6421; Fax: +81-3-5800-6983.

ABSTRACT

We present the single-walled carbon nanotube/silicon (SWNT/Si) solar cells approaching 11% power conversion efficiency (PCE) with the stability of more than six months in air by exploiting the excellent optical, electrical and chemical properties of the pristine randomly oriented SWNTs with very long bundle length. Different from the significant PCE degradation reported in the previous literature, the PCEs of the fabricated solar cells slightly increased after six-month exposure in air without any external protection, making it possible for the SWNT/Si solar cell to extend beyond its energy payback time. Moreover, the fabricated SWNT/Si solar cells also demonstrate sound applicability under low light intensities. The mechanism is discussed by varying the interfacial oxide layer between the SWNTs and Si and modeling the current density-voltage characteristics of SWNT/Si solar cells under different light intensities. The high efficiency and stability demonstrated in this study make SWNT/Si solar cell very promising for practical applications.
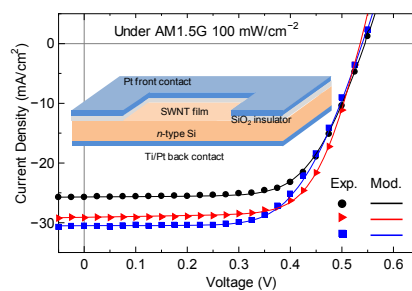
KEYWORDS: Single-walled carbon nanotube, solar cell, high efficiency, stability, SWNT/Si, energy pay back time

Single-walled carbon nanotubes (SWNTs) possess excellent optical,[1] electrical,[2] mechanical and thermal properties[3] as well as chemical stability, hence the capability for multipurpose applications. Especially for the light harvesting application, SWNTs have the superiorities in terms of the wide spectrum of absorption ranging from near-infrared to visible wavelength, high electrical conductivity at high transparency as well as the multiple exciton generation. Combined with earth abundance and chemical stability, the SWNT is supposed to be a very promising candidate for next-generation solar cell applications.[4, 5]

In fact, SWNTs have been investigated intensively for their solar cell applications, and certain achievements and understandings have been reported. Recently, SWNT/Si solar cells are drawing emerging attentions with their power conversion efficiency (PCE) increased by an order of magnitude.[6-16] To date, the SWNT/Si solar cell is the only kind of SWNT-based solar cells with PCE exceeding 10%. Besides the pursuit of the highest peak PCEs, the stability is an even more critical property for assessing the potential applications of solar cells. Actually, the SWNT is one of the most chemically stable materials which could be exploited to protect the solar cells from degradation. However, the so-far-reported peak PCEs of the SWNT/Si solar cells degraded by almost 50% after hours in air, and 20% even with external protection.[8-11] This could be attributed to that the peak PCEs were boosted by nitric acid or gold salt doping which were very instable. The energy payback time (EPBT) of Si-based solar cells ranges from 24 to 48 months.[17-19] For practical applications, the severe degradation in PCE over such a short time is fatal for the SWNT/Si solar cells to reach their EPBT.

In this letter, we utilize the superior optical and electrical properties of the pristine randomly oriented SWNTs as well as their excellent stability for the fabrication SWNT/Si solar cells. The record-high PCE approaching 11% has been achieved for the solar cell sample using the pristine

SWNT film without any chemical treatment. More importantly, the peak PCE is stable for at least six months in air with no external protection. In fact, a slight increase of the PCE value is observed rather than the severe decrease in previous literatures. This duration is expected to further extend beyond the EPBT of the SWNT/Si solar cells. Overall, the fabricated SWNT/Si solar cells with PCEs reaching 11% show significantly higher stability, compared with the previously reported over-10%-PCE solar cells.

The randomly oriented SWNT films with high purity and long bundle length were synthesized by the aerosol CVD method described elsewhere.[20] The ferrocene vapor was thermally decomposed in the gas phase in the aerosol CVD reactor at the temperature of 880 ˚C. The CO gas was supplied at 4 L/min and decomposed on the iron nanoparticles, leading to the growth of SWNTs. The as-synthesized SWNTs were collected by passing the flow through microporous filters at the downstream of the reactor. The transparency of the SWNT films can be varied by changing the collection time. The collected SWNT films can be transferred to arbitrary substrates through the dry transfer process.[20, 21]

In this study, the as-synthesized SWNT films were transferred to fused quartz substrates and subsequently densified by drop-casting approximately 20 μL of ethanol and drying in the ambient environment. From the optical image shown in Figure 1a, it can be observed that the SWNT film is highly transparent at the macroscale. The SEM (Hitachi S-4800) images of the corresponding SWNT films at low and high magnifications are shown in Figure 1b. The SWNT films are well percolated at the microscale with X-junction and Y-junction inter-tube contact.[22] The Raman spectra were measured on a thicker SWNT film to obtain stronger signal. As shown by the Raman spectra (Renishaw inVia) in Figure 1c, the SWNT films have very high crystallinity with the G/D ratio[23] over 30. The radial breathing modes (RBMs) of the Raman

spectra under the excitation laser wavelength of 488, 532, 633 and 785 nm are also given in Figure 1c. The peak RBM intensity positions locate at ca. 120 cm^{-1} to 130 cm^{-1} for all the laser excitation, thus the mean diameter of the SWNTs could be estimated[23] as 2.0 nm ~ 2.1 nm. The mean diameter is further confirmed by the E_{11} position (~2400 nm) from the transmittance spectrum in Figure 1d. As there is no surfactant or sonication process during the film preparation, the high crystallinity, good inter-tube contact and very long bundle length of the SWNTs are well retained. This leads to the high optical transparency and electrical conductivity of the SWNT films as well as the good contact with other materials simultaneously. The sheet resistance (Agilent 4156C; Kyowa-Riken K89PS) and the transmittance (Shimadzu UV-3150) measured at the wavelength of 550 nm (550 nm is the wavelength that has the highest spectral irradiance over the AM1.5G spectrum shown in Figure 1d) for all the pristine SWNT films are listed in Table 1. The TCF samples with the transmittance of around 70%, 80% and 90% are named as TCF70, TCF80 and TCF90, respectively. The sheet resistance is an averaged value measured from -0.5 V to 0.5 V with a measurement step of 5 mV. Table 1 shows that, among the randomly oriented pristine SWNT films reported so far,[24-26] the SWNT films used in this study possess the best trade-off between transparency and conductivity with very high SWNT crystallinity.
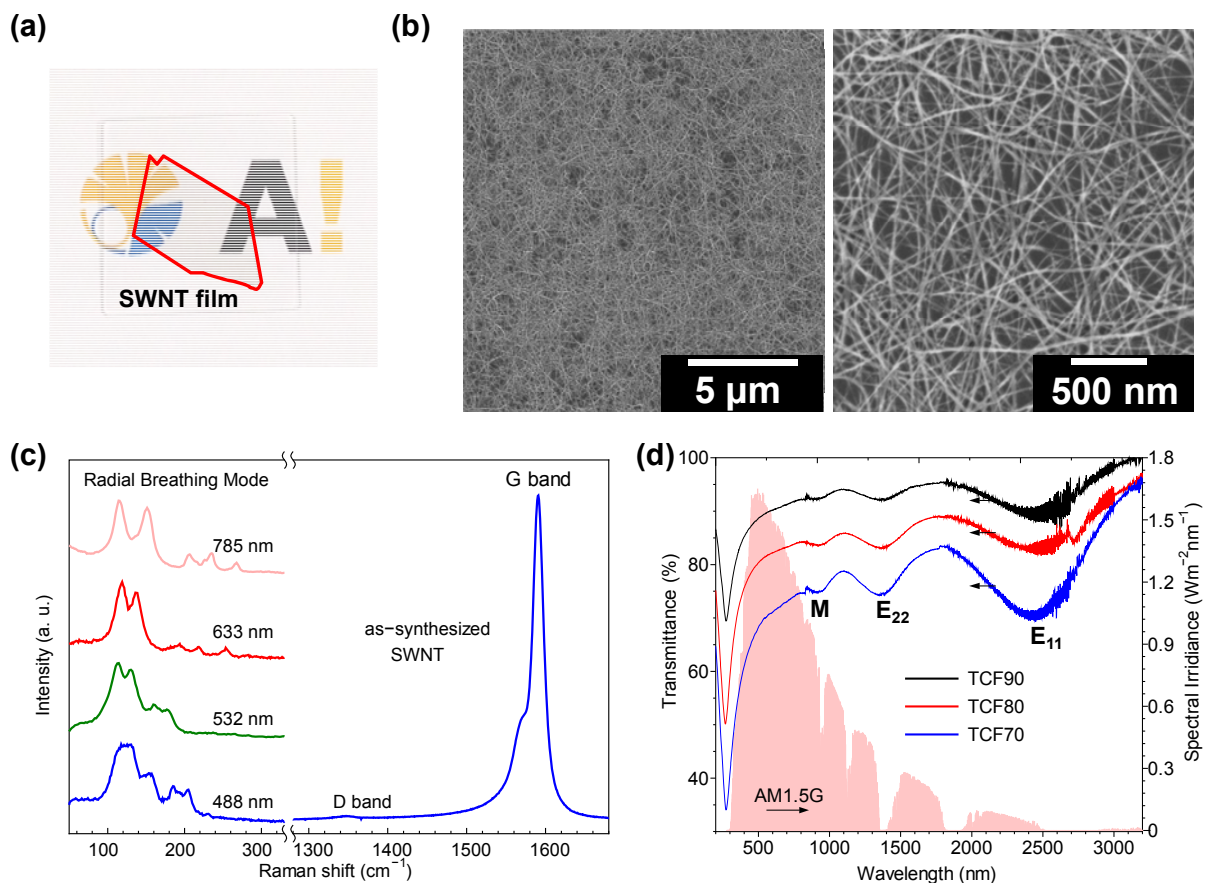
Figure 1. (a) An SWNT film on the fused quartz substrate after the dry-transfer process. (b) The SEM images at the low and high magnifications of the SWNT film from (a). (c) Raman spectra of the SWNT film under the laser excitation with the wavelength of 488 nm, 532 nm, 633 nm and 785 nm. (d) Transmission spectra of the TCF70, TCF80 and TCF90 SWNT films over the wavelength range of 200 nm to 3200 nm, with the background of AM1.5G irradiance spectrum.

Table 1 Optical transmittance (at the wavelength of 550 nm) and sheet resistance (averaged values) of TCF70, TCF80 and TCF90 samples.

Pristine SWNT films	Transmittance (%)	Sheet Resistance (Ω/sq.)
TCF70	70.0	85
TCF80	81.5	134
TCF90	88.8	417
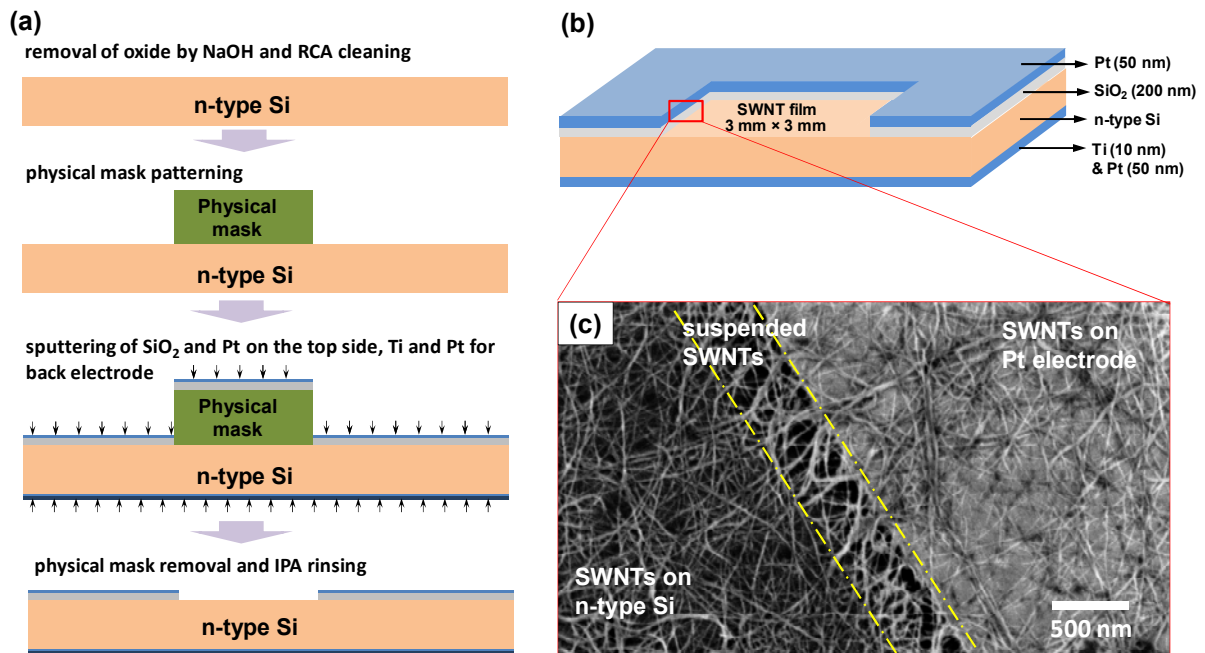
Figure 2. (a) Fabrication process of the *n*-type Si substrate for the SWNT/Si solar cell. (b) Schematic of the SWNT/Si solar cell with dimensional parameters. (c) Magnified SEM image of contact window edge of the SWNT/Si solar cell. A region of the SWNT film with the width of 300 nm was suspended between the Si substrate and the Pt electrode.

Each SWNT/Si solar cell was formed by transferring the SWNT film onto an *n*-type Si substrate. The *n*-type Si (SUMCO Inc.) has the series resistance of 10 ± 2.5 Ω/cm with the dopants concentration of $\sim 10^{15}$ m^{-3}. The fabrication process of the Si substrate for the SWNT-Si solar cell is given in Figure 2a. Before the metal deposition, the *n*-type Si substrate was consequentially treated with RCA1, 5 M NaOH and RCA2 solution for the removal of oxide layer and impurity metals. After the treatment, a very thin oxide layer was formed with the thickness of 6 Å ~7 Å, according to the Si 2p spectrum measured by the X-ray photoelectron spectroscopy (XPS, PHI 5000 VersaProbe) (Supporting Information S1). The 3 mm × 3 mm physical masks were patterned on the top surface of the Si substrate before the metal deposition. A 200-nm-thick SiO$_2$ insulator layer and a 50-nm-thick Pt electrode were subsequently RF-sputtered (ULVAC-RIKO, Inc.) on the top surface of the Si substrate. Ti with the thickness of 10

nm was selected as the back electrode for the lineup of the band structure. The SWNT films were transferred onto the top surface after the removal of the physical masks. The schematic of the fabricated SWNT/Si solar cell with dimensional parameters is shown in Figure 2b. A region of the SWNT film with the width of 300 nm was suspended between the Pt electrode and the Si substrate (Figure 2c), owing to the step formed by the SiO_2 insulator and Pt electrode layers. The size of the suspended region can be ignored in comparison with that of the SWNT/Si contact window.

The current density-voltage (*J-V*) characteristics of the SWNT/Si solar cells using the TCF70, TCF80 and TCF90 films were measured under AM1.5G 100 mW/cm^2 illumination (PEC-L01, Peccell Technologies, Inc.). The results are shown in Figure 3a. The obtained peak PCE values for the solar cells with the TCF70, TCF80 and TCF90 SWNT films are 9.2%, 10.8% and 10.1%, respectively. The PCE of the solar cell using the TCF80 film is the highest among the pristine SWNT/Si solar cells reported so far, and is comparable to the SWNT/Si solar cells doped with nitric acid and/or gold salt in the previous literatures.[8-10, 15, 16] The superiority of PCE over the previous results is attributed to the well-retained high crystallinity, long tube length of the SWNTs as well as the sound inter-SWNT and SWNT-Si contact. The open-circuit photovoltage (V_{oc}), short-circuit photocurrent (J_{sc}), fill factor (FF) and PCE of the fabricated solar cells are listed in Table 2. The J_{sc} values of the solar cell samples with the TCF70, TCF80 and TCF90 films were 25.7, 29.5 and 30.9 mA/cm^2, respectively. Theoretically, higher transmittance would allow more solar irradiation on the SWNT/Si interface, hence the higher photocurrent. However, the photocurrents of the fabricated solar cells do not vary linearly with the transparency of the SWNT films. This could be attributed to the less contribution from the SWNTs part, owing to the decreased light absorbance of SWNTs. In addition, the light reflection from the mirror-like Si surface becomes notable when the transmittance of the SWNT film is very high.

The *J-V* characteristics of the SWNT/Si solar cells under the dark condition are shown in Figure 3b. The rectification ratio of 1 V to -1 V is more than ~10^3, which demonstrates the excellent diode behavior of the SWNT/Si junction. The ideality factors are calculated as the slopes of the *J-V* curves in the logarithm scale ranging from 0.4 V to 0.6V, which are 1.7, 2.1 and 2.2 of the solar cells using the TCF70, TCF80 and TCF90 films, respectively. Moreover, with the aim of testing the reproducibility of the fabricated solar cell, four solar cell samples using the TCF80 films, *i.e.*, TCF80-A, TCF80-B, TCF80-C and TCF80-D, were compared in Figure 3c. The uncertainties of the V_{oc}, J_{sc}, FF and PCE are within 2.5 mV, 0.2 mA/cm^2, 0.005 and 0.15%, respectively, demonstrating the high reproducibility of the solar cell performance. The four above-mentioned solar cells samples used for the comparison are from the same batch of fabrication to guarantee the credibility and comparability. The experimental fluctuations among different batches of fabrication are also very small, as discussed in Supporting Information S2.

Besides the peak PCE value, the stability is an even more important criterion for evaluating an emerging solar cell. In this research, we rendered the outstanding chemical stability of the pristine SWNTs to realize a steady and highly efficient solar cell output without any external protection. As shown in Figure 3d, the *J-V* characteristics underwent almost no change in the six-month duration. Actually, both the FF and PCE values slightly increased, owing to the oxygen modification to SWNT films, which would *p*-dope SWNTs and make the SWNT films more conductive (Supporting Information S3).[27] It is expected that this stability record will further extend beyond the EPBT, making it possible for the practical applications of the SWNT/Si solar cells. This is, to our knowledge, the only stable over-10%-PCE SWNT/Si solar cell reported so far. In fact, the high-quality pristine SWNTs used in the present study are inherently much more stable than sealing techniques such as PDMS coating. Moreover, applying

the TiO_2 antireflection layer could harvest up to 30% solar energy which was reflected by the mirror-like Si surface.[11, 13] It is worth mentioning that no external techniques have been employed so far. We believe that a stable and even higher PCE would be achieved by utilizing TiO_2 coating technique to the current SWNT/Si solar cells.
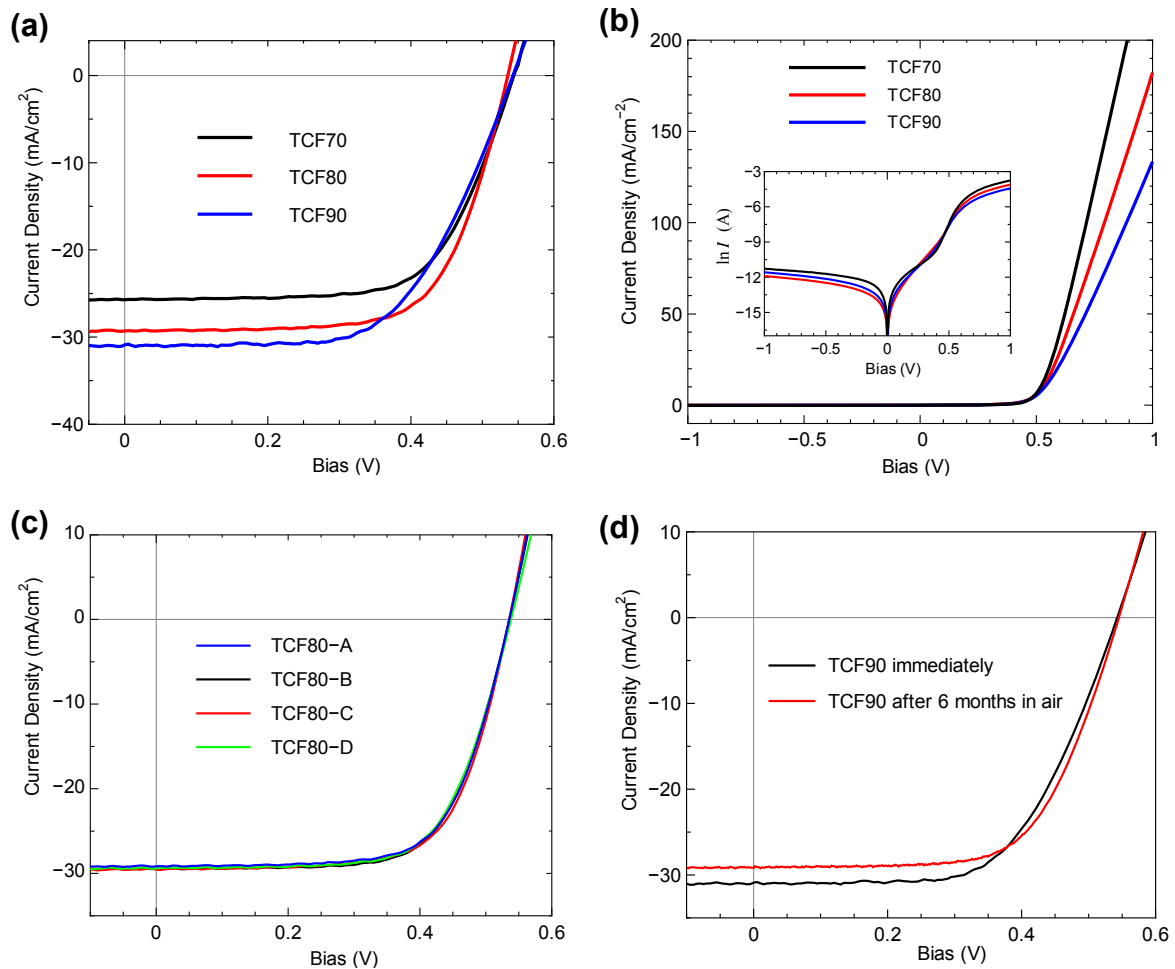
Figure 3. (a) Representative *J-V* characteristics of the SWNT/Si solar cells with the TCF70, TCF80 and TCF90 films under 100 mW/cm^2 AM1.5G illumination. (b) *J-V* characteristics of the SWNT/Si solar cells under the dark condition. (c) Reproducibility of *J-V* characteristics of four solar cell samples with the TCF80 films fabricated in one batch. (d) *J-V* characteristics of two solar cells with the TCF90 films measured immediately after fabrication and after six months in air without any external protection.

In practical applications, the light intensity varies by many factors and is usually lower than 100 mW/cm^2 used in the standard solar test. The decrease of the light intensity would result in the decreases of J_{sc} and V_{oc}. The J_{sc} varies proportionally to the light intensity and thus will not actually affect the PCE. However, the degradation of V_{oc} resulted from the decrease of the light intensity will reduce the PCE.[28, 29] Therefore, the V_{oc} of the solar cell under the light intensity of lower than 100 mW/cm^2 is another important parameter characterizing the quality of the solar cell. In this research, the dependency of the V_{oc} of the SWNT/Si solar cells using the TCF90 films on the light intensities was studied. As shown in Figure 4a, the V_{oc} experienced only a 10% drop from 540 to 460 mV (measurement uncertainty was 2.5 mV) when the light intensity decreased from 100 to 10 mW/cm^2. Figure 4b shows the J-V characteristics of the SWNT/Si solar cells using the TCF90 films measured under the illumination of 100, 78, 50 and 20 mW/cm^2. The PCE value of the solar cell only decreased slightly with the decrease of the light intensity, making it suitable for the applications under low light intensity.

The curve fitting to the experimental J-V characteristics of the solar cells is an insightful method for the in-depth investigation of the solar cell performance. In this research, the equivalent circuit shown in the inset of Figure 4a was used to model the operation of the SWNT/Si solar cells. The corresponding p-n diode equation is expressed as

$$I = I_{sc} - I_0 \exp\left[\frac{q(V + IR_S)}{nkT} \right] - \frac{V + IR_S}{R_{SH}} \tag{1}$$

where n is the ideality factor, I_0 is the dark saturation current, kT/q is the thermal voltage, I_{sc} is the short-circuit current, R_S is the series resistance and R_{SH} is the shunt resistance.[30] The I_0 is discussed in details in the Supporting Information S4. When the current I in the Equation (1) equals zero, the V_{oc} can be obtained as

$$V_{oc} = \frac{nkT}{q} \ln\left[\frac{I_{sc} - \left(V_{oc} \middle/ R_{SH} \right)}{I_0} \right] \qquad (2)$$

when R_{SH} is comparable to the V_{oc}/I_{sc}, an additional loss of the V_{oc} would be induced under low light intensity. If the R_{SH} in the Equation (2) is sufficiently large, the ideal V_{oc} model can be approximated as

$$V_{oc} = \frac{nkT}{q} \ln\left[\frac{I_{sc}}{I_0} \right] \qquad (3)$$

As shown in Figure 4a, the experimental dependency of V_{oc} on the light intensities can be well fitted by the ideal V_{oc} model, which demonstrates that the R_{SH} of the solar cell is large enough for the light intensities ranging from 100 to 10 mW/cm^2. Therefore, the SWNT/Si solar cells in this study have sound operation applicability under low light intensities.

To further investigate the effects of R_S and R_{SH}, the equivalent circuit model was also used to fit the *J-V* curves of the fabricated SWNT/Si solar cells measured under different light intensities, aiming at extracting the R_S and R_{SH}. As shown in Figure 4b, the *J-V* curves of the SWNT/Si solar cell using the TCF90 film under different light intensities were all well fitted by the *p-n* diode solar cell model. The obtained R_S and R_{SH} of the solar cell using the TCF90 film were calculated as 33.8 Ω and more than 20 kΩ, respectively. The curve fitting results of the *J-V* characteristics of the SWNT/Si solar cells with the TCF70 and TCF80 films are also shown in Figure 4c. The calculated R_S for the SWNT/Si solar cells using the TCF70 and TCF80 films have the same value of 27.5 Ω. The obtained R_{SH} for these two solar cell samples were also more than 20 kΩ.

The obtained R_S, R_{SH} and I_0 for the SWNT/Si solar cells using the TCF70, TCF80 and TCF90 films are listed in Table 2.

The R_S and R_{SH} determine the quality of a solar cell, *i.e.*, FF, which is one of the three parameters characterizing solar cell performance along with J_{sc} and V_{oc}. The FF values for the SWNT/Si solar cells using the TCF70, TCF80 and TCF90 films were 68%, 68% and 61%, respectively. As discussed above, the effect of R_{SH} on the performance of the solar cells is ignorable. The R_S is composed of four factors, *i.e.*, the SWNT film-electrode contact, the sheet resistance of the SWNT film, the resistance of Si substrate and the resistance of electrode. Except for the sheet resistance of the SWNT film, the three factors are inherent and can be considered the same in one fabrication batch. As the TCF90 has the highest sheet resistance among all the films, the solar cell using the TCF90 film has much lower FF. However, the SWNT/Si solar cells with the TCF70 and TCF80 films have the same R_S and FF, although the sheet resistance of the TCF70 film is lower than that of the TCF80 film. This means that when the sheet resistance of the SWNT film is as low as 100 Ω/sq., the inherent resistance of the solar cell architecture becomes dominant. The FFs of the solar cells using the randomly oriented films in this study were limited to 68% for all the solar cell samples, owing to the device architecture. Previously, we have reported a record-high FF up to 72% using a microhoneycomb-networked SWNTs,[15] in which micro-grids made of dense SWNT walls significantly reduced the carrier diffusion length from millimeter-scale to micrometer-scale.

We further investigate the effect of interfacial oxide layer on the performance of the SWNT/Si solar cells. For the Schottky-barrier Si solar cells, it has been well studied that inserting an oxide layer with the thickness of 13 ~ 20 Å between the metal and semiconductor would improve the solar cell performance by eliminating the pinning of the Fermi level.[31-33] This theory was used to

partially explain the substantial increase of PCE by adding nitric acid or other strong oxidants to SWNT/Si solar cells which were then considered as Schottky-barrier solar cells. In this study, we designed an experiment to verify this hypothesis. The TCF70 SWNT films were used for fabricating two kinds of SWNT/Si solar cell with different oxide layer thicknesses, as the TCF70 SWNT films possess the highest electrical conductivity among all the TCF films used in this research, which could best simulate metal layer in Schottky solar cells. The two Si substrates with different thicknesses of oxide layers were prepared by varying the treatment time of RCA2 cleaning. The Si substrate treated by the RCA2 solution for 5 s was utilized for the fabrication of the TCF70 solar cell sample which has the above-mentioned performance (Figure 3a and 3b), while the Si substrate treated for 3 min was used for the OxideTCF70 solar cell sample (Figure 4d). According to the Si 2p XPS spectrum (Supporting Information S2), the oxide thickness of the Si substrate for the TCF70 solar cell sample was calculated as 6.9 Å which was approximately the limit of the native oxide layer grown in air.[34-36] In the case of the Si substrate for the OxideTCF70 solar cell sample, the 3-min RCA2 cleaning would leave an oxide layer with the thickness of 13 ~ 15 Å, which has been thoroughly investigated in the previous literatures.[37, 38] As shown in Figure 4d, the PCE, FF and V_{oc} of the OxideTCF70 solar cell sample were significantly lower than those of the TCF70 solar cell sample. The photocurrent degradation near the V_{oc} is attributed to the increase of series resistance between the SWNT film and Si substrate. Moreover, in the case of the OxideTCF70 solar cell, the thick oxide layer between the SWNT film and the Si substrate serves as a capacitor. The hysteresis between the forward and reverse scans of OxideTCF70 solar cell sample results from the charging and discharging of the dielectric layer. This experimental result serves as an indirect evidence of the insufficiency of the MIS mechanism of the SWNT/Si solar cells fabricated in this research. The

SWNT/Si solar cell is different from the conventional metal-insulator-semiconductor (MIS) junction.
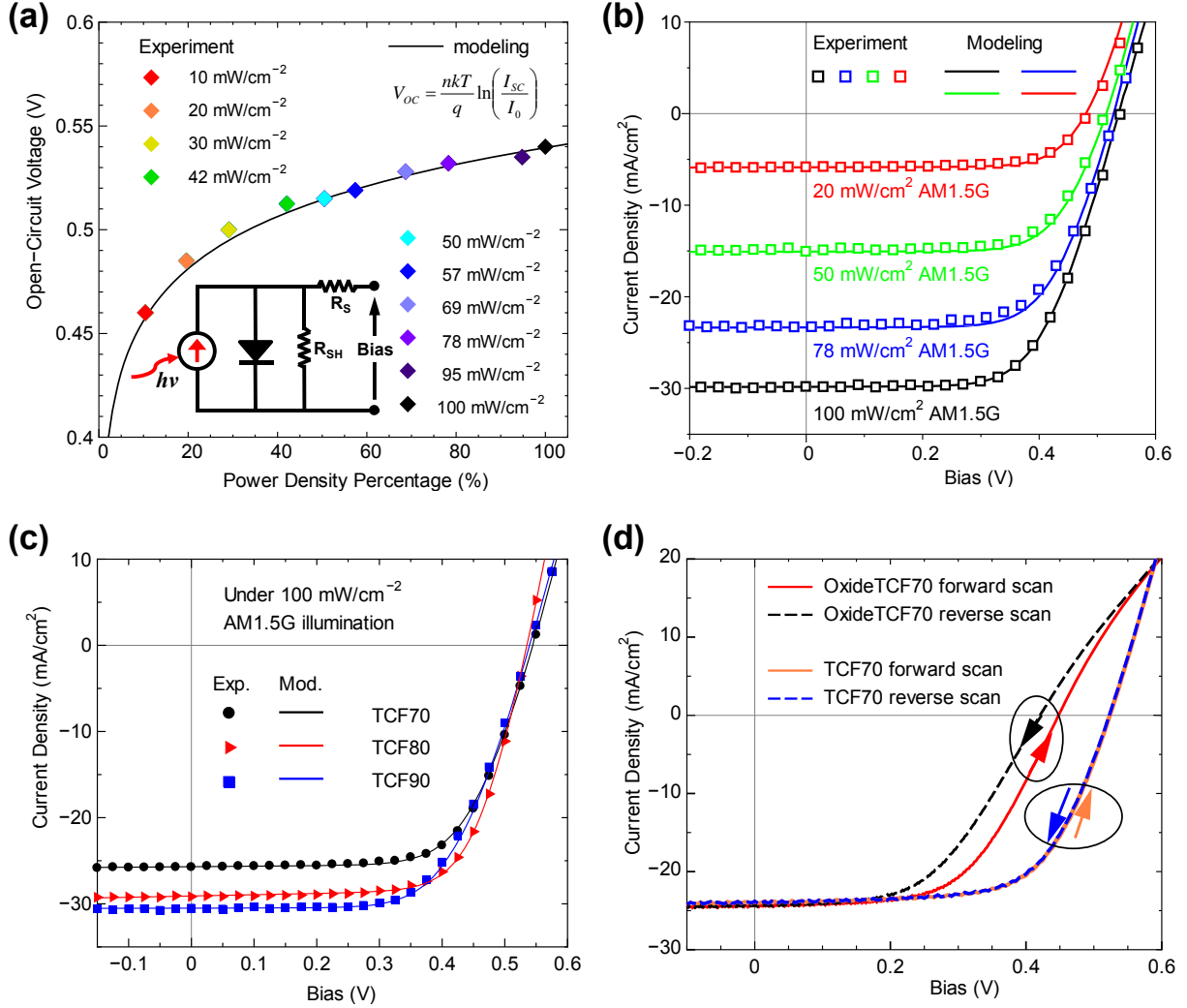
Figure 4. (a) The dependency of open-circuit voltage on light intensity. The black line is the modeling result of this dependency. The inset is the equivalent circuit of the SWNT/Si solar cells. (b) *J-V* characteristics of the SWNT/Si solar cells under different light intensities. The symbols denote the experimental results, while the lines represent the modeling results by the *p-n* diode equation. (c) The curve fitting of the *J-V* characteristics of the SWNT/Si solar cells using the TCF70, TCF80 and TCF90 films. (d) Hysteresis of the forward and reverse scans for the OxideTCF70 and the TCF70 samples which respectively have the oxide layers with the thicknesses of around 15 Å and 7 Å between the SWNT film and Si substrate.

Table 2 The power conversion efficiency (PCE), fill factor (FF), short-circuit current (J_{sc}) and open-circuit voltage (V_{oc}) of the SWNT/Si solar cells with the TCF70, TCF80 and TCF90 films measured immediately after fabrication, and those of the solar cell with TCF90 film measured 6 months after fabrication, as well as the series resistance (R_S), the shunt resistance (R_{SH}) and dark saturation current (I_0) through *p-n* diode equation modeling.

Films		Time of Measurement	PCE (%)	FF (-)	J_{sc} (mA/cm^2)	V_{oc} (mV)	R_S (Ω)	R_{SH} (kΩ)	I_0 (pA)
		Experimental Results					Modeling Results		
TCF70			9.3	0.68	25.7	535	27.5	>20	635
TCF80	A		10.6	0.68	29.3	535	-	-	-
	B	Immediately	10.7	0.67	29.6	535	-	-	-
	C		10.8	0.68	29.7	535	27.5	>20	144
	D		10.6	0.67	29.6	535	-	-	-
TCF90			10.1	0.61	30.9	535	33.8	>20	847
		6 Months in Air	10.2	0.64	29.2	540	-	-	-

In summary, we have demonstrated the air-stable SWNT/Si solar cells with PCE approaching 11% for the first time. The PCE of the solar cells slightly increases after half a year and is expected to reach the EPBT of the fabricated solar cell. Compared with previously reported results, the fabricated solar cells show a significantly higher stability. The experimental results are well fitted by the *p-n* diode equation model and the mechanisms of the improved performance of the SWNT/Si solar cells are discussed accordingly. We believe that the full exploitation of the superior electrical, optical and chemical properties of SWNTs is very promising for the next generation photovoltaic devices.

ACKNOWLEDGMENTS

Supporting Information Available: X-ray photoelectron spectroscopy of the Si substrate used in the SWNT/Si solar cells, performance fluctuation for the solar cells fabricated in different batches, resonant Raman spectroscopy of the SWNT films, dark saturation current of the SWNT/Si solar cells, spectral response of the SWNT/Si solar cells in the UV and visible light spectrum. This material is available free of charge via the Internet at http://pubs.acs.org.

REFERENCES

(1)   Avouris, P.; Freitag, M.; Perebeinos, V. *Nat. Photonics* **2008,** 2, 341-350.

(2)   Jariwala, D.; Sangwan, V. K.; Lauhon, L. J.; Marks, T. J.; Hersam, M. C. *Chem. Soc. Rev.* **2013,** 42, 2824-2860.

(3)   Marconnet, A. M.; Panzer, M. A.; Goodson, K. E. *Rev. Mod. Phys.* **2013,** 85, 1295-1326.

(4)   Baughman, R. H.; Zakhidov, A. A.; de Heer, W. A. *Science* **2002,** 297, 787-792.

(5)   De Volder, M. F. L.; Tawfick, S. H.; Baughman, R. H.; Hart, A. J. *Science* **2013,** 339, 535-539.

(6)   Wei, J.; Jia, Y.; Shu, Q.; Gu, Z.; Wang, K.; Zhuang, D.; Zhang, G.; Wang, Z.; Luo, J.; Cao, A.; Wu, D. *Nano Lett.* **2007,** 7, 2317-2321.

(7)   Jia, Y.; Wei, J.; Wang, K.; Cao, A.; Shu, Q.; Gui, X.; Zhu, Y.; Zhuang, D.; Zhang, G.; Ma, B.; Wang, L.; Liu, W.; Wang, Z.; Luo, J.; Wu, D. *Adv. Mat.* **2008,** 20, 4594-4598.

(8)   Jia, Y.; Li, P.; Gui, X.; Wei, J.; Wang, K.; Zhu, H.; Wu, D.; Zhang, L.; Cao, A.; Xu, Y. *Appl. Phys. Lett.* **2011,** 98, -.

(9)   Jia, Y.; Cao, A.; Bai, X.; Li, Z.; Zhang, L.; Guo, N.; Wei, J.; Wang, K.; Zhu, H.; Wu, D.; Ajayan, P. M. *Nano Lett.* **2011,** 11, 1901-1905.

(10)   Jung, Y.; Li, X.; Rajan, N. K.; Taylor, A. D.; Reed, M. A. *Nano Lett.* **2012,** 13, 95-99.

(11)   Shi, E.; Zhang, L.; Li, Z.; Li, P.; Shang, Y.; Jia, Y.; Wei, J.; Wang, K.; Zhu, H.; Wu, D.; Zhang, S.; Cao, A. *Sci. Rep.* **2012,** 2.

(12)   Wadhwa, P.; Liu, B.; McCarthy, M. A.; Wu, Z.; Rinzler, A. G. *Nano Lett.* **2010,** 10, 5001-5005.

(13)   Shi, E.; Li, H.; Yang, L.; Zhang, L.; Li, Z.; Li, P.; Shang, Y.; Wu, S.; Li, X.; Wei, J.; Wang, K.; Zhu, H.; Wu, D.; Fang, Y.; Cao, A. *Nano Lett.* **2013,** 13, 1776-1781.

(14)   Wadhwa, P.; Seol, G.; Petterson, M. K.; Guo, J.; Rinzler, A. G. *Nano Lett.* **2011,** 11, 2419-2423.

(15)   Cui, K.; Chiba, T.; Omiya, S.; Thurakitseree, T.; Zhao, P.; Fujii, S.; Kataura, H.; Einarsson, E.; Chiashi, S.; Maruyama, S. *J. Phys. Chem. Lett.* **2013,** 4, 2571-2576.

(16)   Tune, D. D.; Flavel, B. S.; Krupke, R.; Shapter, J. G. *Adv. Energy Mat.* **2012,** 2, 1043-1055.

(17)   Espinosa, N.; Hosel, M.; Angmo, D.; Krebs, F. C. *Energy Environ. Sci.* **2012,** 5, 5117-5132.

(18)   Fthenakis, V.; Alsema, E. *Prog. Photovoltaics: Res. Appl.* **2006,** 14, 275-280.

(19)   Mann, S. A.; de Wild-Scholten, M. J.; Fthenakis, V. M.; van Sark, W. G. J. H. M.; Sinke, W. C. *Prog. Photovoltaics: Res. Appl.* **2013**, DOI: 10.1002/pip.2363.

(20)   Kaskela, A.; Nasibulin, A. G.; Timmermans, M. Y.; Aitchison, B.; Papadimitratos, A.; Tian, Y.; Zhu, Z.; Jiang, H.; Brown, D. P.; Zakhidov, A.; Kauppinen, E. I. *Nano Lett.* **2010,** 10, 4349-4355.

(21)   Nasibulin, A. G.; Kaskela, A.; Mustonen, K.; Anisimov, A. S.; Ruiz, V.; Kivistö, S.; Rackauskas, S.; Timmermans, M. Y.; Pudas, M.; Aitchison, B.; Kauppinen, M.; Brown, D. P.; Okhotnikov, O. G.; Kauppinen, E. I. *ACS Nano* **2011,** 5, 3214-3221.

(22)   Sun, D.-m.; Timmermans, M. Y.; Tian, Y.; Nasibulin, A. G.; Kauppinen, E. I.; Kishimoto, S.; Mizutani, T.; Ohno, Y. *Nat. Nanotechnol.* **2011,** 6, 156-161.

(23)   Dresselhaus, M. S.; Dresselhaus, G.; Saito, R.; Jorio, A. *Phys. Rep.* **2005,** 409, 47-99.

(24)   Geng, H.-Z.; Kim, K. K.; So, K. P.; Lee, Y. S.; Chang, Y.; Lee, Y. H. *J. Am. Chem. Soc.* **2007,** 129, 7758-7759.

(25)   Mirri, F.; Ma, A. W. K.; Hsu, T. T.; Behabtu, N.; Eichmann, S. L.; Young, C. C.; Tsentalovich, D. E.; Pasquali, M. *ACS Nano* **2012,** 6, 9737-9744.

(26)   Wu, Z.; Chen, Z.; Du, X.; Logan, J. M.; Sippel, J.; Nikolou, M.; Kamaras, K.; Reynolds, J. R.; Tanner, D. B.; Hebard, A. F.; Rinzler, A. G. *Science* **2004,** 305, 1273-1276.

(27)   Collins, P. G.; Bradley, K.; Ishigami, M.; Zettl, A. *Science* **2000,** 287, 1801-1804.

(28)   Bunea, G. E.; Wilson, K. E.; Meydbray, Y.; Campbell, M. P.; De Ceuster, D. M. In 4th World Conference on Photovoltaic Energy Conversion, May 2006, 2006; 2006; pp 1312-1314.

(29)   Rodrigo, P.; Rus, C.; Almonacid, F.; Pérez-Higueras, P. J.; Almonacid, G. *Sol. Energy Mater. Sol. Cells* **2012,** 96, 186-194.

(30)   Wang, F.; Kozawa, D.; Miyauchi, Y.; Hiraoka, K.; Mouri, S.; Matsuda, K. *Appl. Phys. Express* **2013,** 6, 122301.

(31)   Lillington, D. R.; Townsend, W. G. *Appl. Phys. Lett.* **1976,** 28, 97-98.

(32)   Shewchun, J.; Singh, R.; Green, M. A. *J. Appl. Phys.* **1977,** 48, 765-770.

(33)   Esposito, D. V.; Levin, I.; Moffat, T. P.; Talin, A. A. *Nat. Mater.* **2013,** 12, 562-568.

(34)   Mende, G. *Surf. Sci.* **1983,** 128, 169-175.

(35)   Morita, M.; Ohmi, T.; Hasegawa, E.; Kawakami, M.; Ohwada, M. *J. Appl. Phys.* **1990,** 68, 1272-1281.

(36)   Engel, T. *Surf. Sci. Rep.* **1993,** 18, 93-144.

(37)   Henderson, R. C. *J. Electrochem. Soc.* **1972,** 119, 772-775.

(38)   Kern, W. *J. Electrochem. Soc.* **1990,** 137, 1887-1892.

Supporting Information

Air-Stable High-Efficiency Solar Cells Using

Improved Single-Walled Carbon Nanotube Films

Kehang Cui,[1] Anton S. Anisimov,[3] Takaaki Chiba,[1] Shunjiro Fujii,[4] Hiromichi Kataura,[4] Albert G. Nasibulin,[2] Shohei Chiashi,[1] Esko I. Kauppinen,[2] Shigeo Maruyama[1]

[1] Department of Mechanical Engineering, The University of Tokyo, Bunkyo-ku, Tokyo 113-8656, Japan

[2] Department of Applied Physics, Aalto University School of Science, Aalto FI-00076, Finland

[3] Canatu Ltd., Konalankuja 5, FI-00390 Helsinki, Finland

[4] Nanosystem Research Institute, National Institute of Advanced Industrial Science and Technology, Tsukuba 305-8562, Japan

Corresponding Author:

Shigeo Maruyama, maruyama@photon.t.u-tokyo.ac.jp,
Department of Mechanical Engineering, The University of Tokyo, 7-3-1 Hongo, Tokyo, 113-8656, Japan; Tel: +81-3-5841-6421; Fax: +81-3-5800-6983.

S1. X-ray photoelectron spectroscopy of the Si substrate used in the SWNT/Si solar cell

X-ray photoelectron spectroscopy was employed to characterize the oxide thickness of the Si substrate used in the SWNT/Si solar cells. Figure S1 shows the Si 2p spectrum. The thickness of the oxide layer d_{ox} could be precisely calculated as

$$d_{ox} = \lambda_{ox} \sin\theta \ln\left(\frac{I_{ox}}{\beta I_{Si}} + 1 \right)$$

where λ_{ox} is the attenuation length of the Si 2p photoelectrons in SiO$_2$, θ is the photoelectron take-off angle, β is the Si 2p intensity ratio of infinitely thick SiO$_2$ and Si ($I_{oxide}^{\infty} \big/ I_{Si}^{\infty}$), and $I_{ox} \big/ I_{Si}$ is the intensity ratio of the measured SiO$_2$ layer and the Si substrate.[S1] In this research, the photoelectron take-off angle θ is $\pi/4$, λ_{ox} and β are well-studied constants and refered from Ref. S1. The calculated thickness of the oxide layer is 6.9 Å. This oxide layer is slightly thinner than the native oxide grown in air.
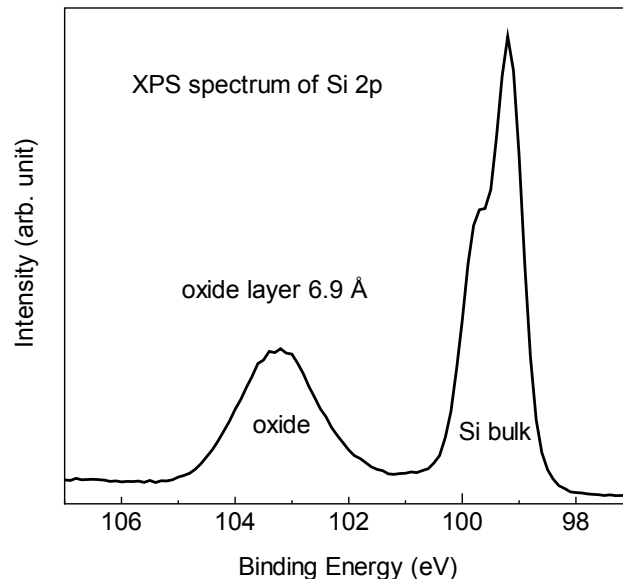
Figure S1. X-ray photoelectron spectroscopy of the Si substrate used in the SWNT/Si solar cell.

S2. Performance fluctuation for the solar cells fabricated in different batches

In the experiments, the experimental uncertainties and fluctuations are inevitable. Figure S2 shows more than 200 *J-V* curves of the fabricated SWNT/Si solar cells. The stable fabrication process and the uniformity of the SWNT film limit the experimental fluctuations in a very low level. The occurrence probability of the low-quality SWNT/Si solar cells is very small (lower than 10%). Such a high reproducibility is very beneficial for the practical applications of the SWNT/Si solar cells.
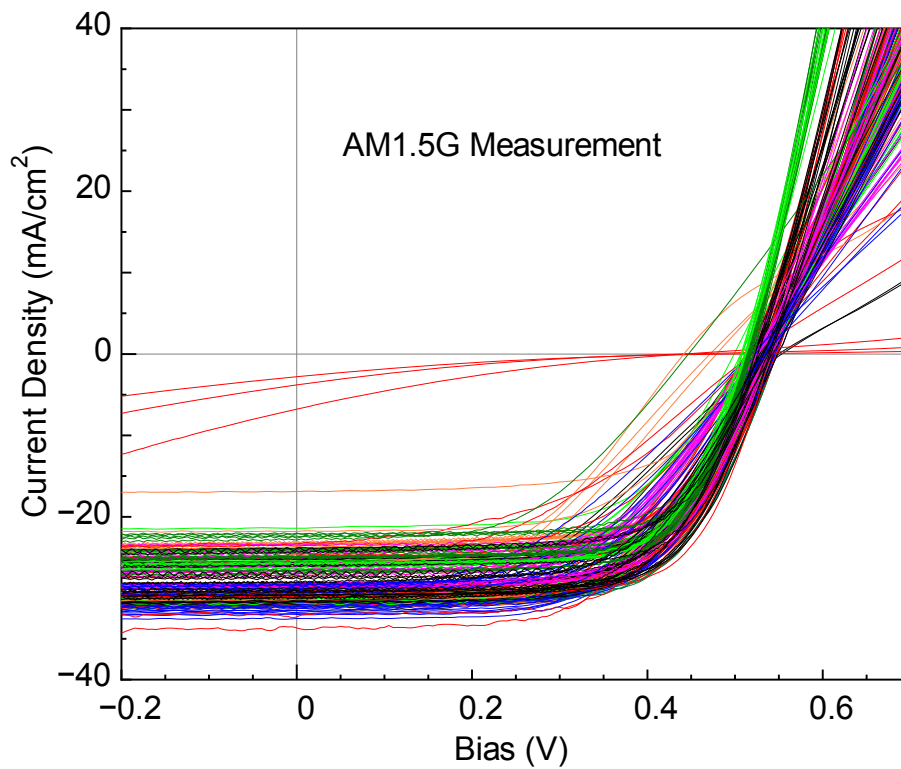
Figure S2. More than 200 *J-V* curves of the SWNT/Si solar cell samples fabricated in different batches.

S3. Resonant Raman spectroscopy of the SWNT films

Resonance Raman spectra were measured to characterize and compare the as-synthesized SWNTs and the SWNTs exposed in air for six months. The spectra were measured with a 488 nm excitation laser incident normal to the substrate. The as-synthesized SWNTs have a very high crystallinity with the G/D ratio over 30. After the six-month exposure in air, the intensity of G band of the initial SWNTs was weakened and the peak position of G band was blue-shifted by 2.1 cm^{-1} from 1590.9 cm^{-1} to 1593.0 cm^{-1}, as shown in the inset of Figure S3. This may be attributed to the charge transfer induced by the oxygen exposure during the six months.
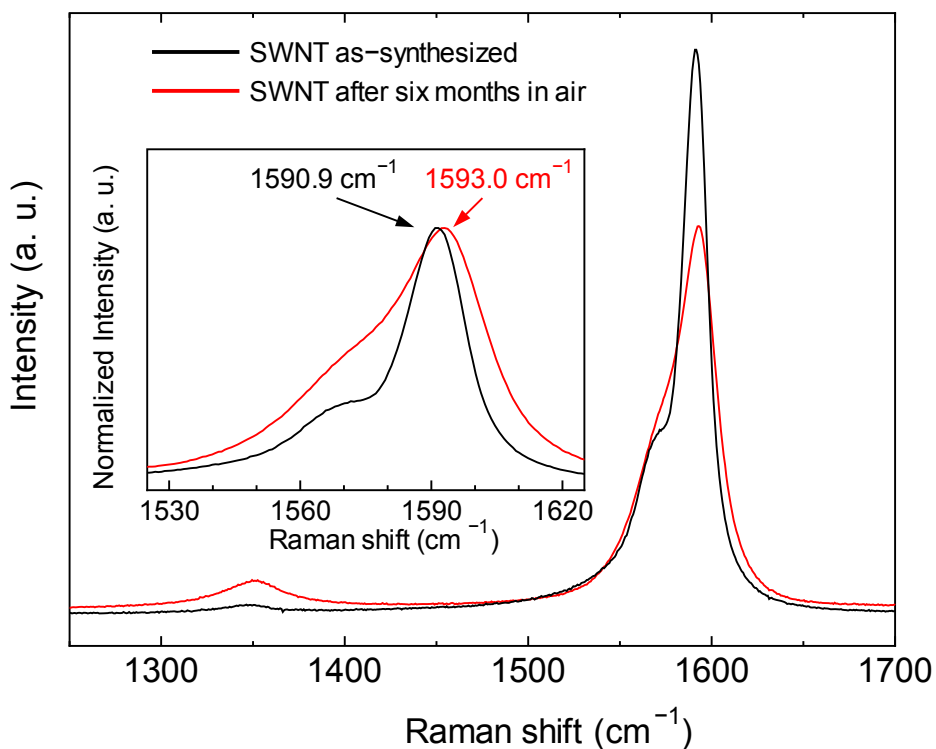
Figure S3. Resonance Raman spectra of the as-synthesized SWNTs and the SWNTs exposed in air for six months. All spectra were measured with a 488 nm excitation laser incident normal to the substrate.

S4. Curve fitting of *J-V* characteristics of SWNT/Si solar cells

Through the curve fitting of the *J-V* characteristics of the SWNT/Si solar cells measured under dark current, the dark saturation current I_0 could be obtained. For an actual *p-n* diode solar cell, the model of the *J-V* characteristics under dark condition is given as[S2]

$$I = I_0 \left(e^{\frac{qV}{nkT}} - 1 \right)$$

where *kT/q* is the thermal voltage which is a constant with the value of 25.85 mV at room temperature; *n* is the ideality factor; and I_0 is the dark saturation current. In this research, this p-n diode equation was utilized to calculate I_0. The obtained I_0 for the SWNT-Si solar cells using the TCF70, TCF80 and TCF90 films are calculated as 6.35×10^{-10} A, 1.44×10^{-10} A and 8.47×10^{-10} A, respectively.

S5. Spectral response of the SWNT/Si solar cells in the UV and visible light spectrum

Figure S5 gives the spectral responses (SM-250TF, Bunkou Keiki Co. Ltd) of the SWNT-Si solar cells and the reference Si *p-n* junction solar cell (Si photodiode S1337, Hamamatsu Photonics K.K.). The difference of the spectral response between the Si *p-n* solar cell and the SWNT/Si solar cells is negligible in the wavelength ranging from 300 nm to 1100 nm. In this wavelength range, the main contribution of photocurrent comes from the Si side in each SWNT/Si solar cell.
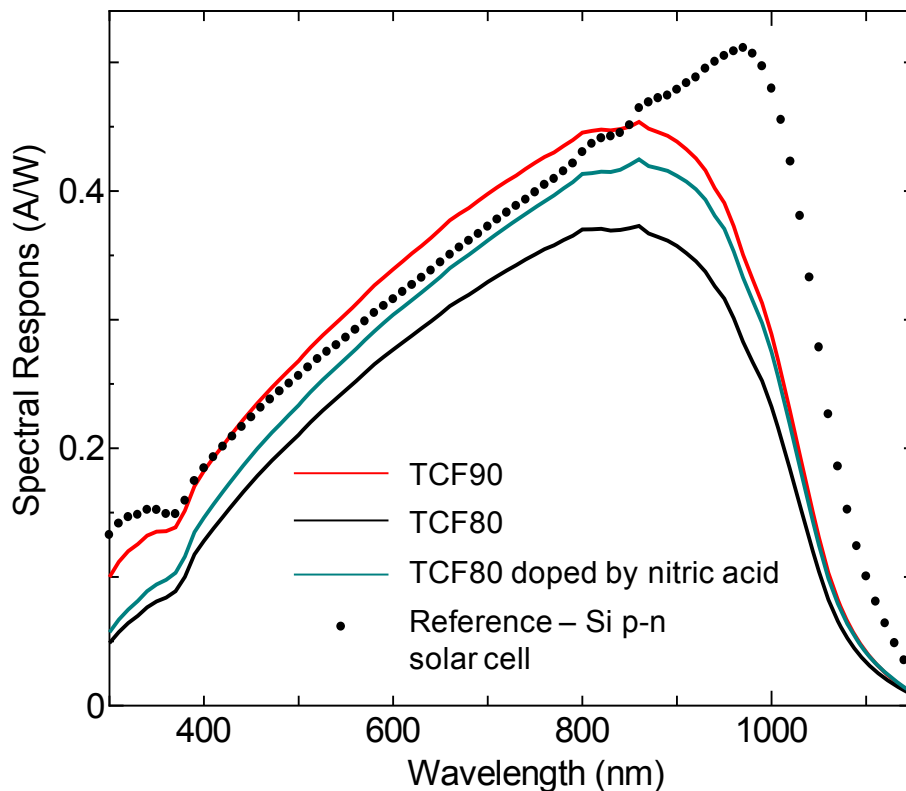
Figure S5. Spectral responses of the reference Si *p-n* solar cell as well as the SWNT/Si solar cells with the TCF90 film, TCF80 film and the TCF80 film doped with nitric acid.

Reference

S1. Liu, Z. H.; McCaffrey, J. P.; Brar, B.; Wilk, G. D.; Wallace, R. M.; Feldman, L. C.; Tay, S. P. *Appl. Phys.Lett.* **1997**, *71*, 2764.

S2. Wurfel, P. Physics of Solar Cells: From Principles to New Concepts, Wiley-WCH Weinheim, 2005.